Nitrous oxide decomposition active site on Ni–MgO catalysts characterized by X-ray absorption fine structure spectroscopy

Yasuo Izumi,* Takehiro Shimizu, Takaaki Kobayashi and Ken-ichi Aika

Department of Environmental Chemistry and Engineering, Interdisciplinary Graduate School of Science and Engineering, Tokyo Institute of Technology, 4259 Nagatsuta, Midori-ku, Yokohama 226-8502, Japan. E-mail: yizumi@chemenv.titech.ac.jp

A contracted Ni^{2+} coordination site distorted in the direction of Ni$\cdots$Mg and Ni$\cdots$Ni was found to be responsible for catalytic N_2O decomposition when Ni^{2+} is diluted in a MgO matrix (Ni^{2+}/Mg^{2+} atomic ratio $\approx$ 1.0) based on a local structure study by nickel K-edge X-ray absorption fine structure spectroscopy.

Nitrous oxide is one of the gases which affects the environment. Catalysts for nitrous oxide decomposition have not been well developed compared with various catalysts for nitric oxide decomposition.[1] Nickel–MgO[2] and cobalt–MgO[3,4] are reported to form solid solutions. Metal ion-exchanged zeolites have been reported to be unstable to the effects of formed water during NO or N_2O decomposition reactions. A thermally and water-stable Co–MgO solid solution has been applied to N_2O decomposition.[4] The formation of an fcc structure-based solid solution was demonstrated by EXAFS (extended X-ray absorption fine structure) within the range of Co atom% [*i.e.* Co/(Co + Mg) $\times$ 100] of 0–5. However, a severe decrease of catalyst surface area and activity was found when the cobalt content exceeded *ca.* 10 atom% owing to the formation of the Co_3O_4 spinel phase.[4] Herein, the structure of Ni–MgO catalysts was investigated by EXAFS, XANES (X-ray absorption near-edge structure) and XRD (X-ray diffraction). Solid solution formation and the correlation between the local coordination structure of Ni ions and N_2O decomposition reactivity are discussed.

Powders were prepared by the impregnation of nickel nitrate into MgO and were heated in air at 1173 K for 24 h and in H_2 at 573 K for 1 h. With increase of nickel concentration, the BET surface area monotonously decreased from 50 m^2 g^{-1} (MgO) to 14 m^2 g^{-1} (Ni–MgO, Ni 33.6 atom%) and then remained constant upon further increase of nickel content. The decomposition of N_2O (0.1%) in helium (balance to 101.3 kPa) was monitored at 873 K in a flow system (flow rate 100 ml min^{-1}, 0.2 g catalyst used). The steady-state formation rate of N_2 (and O_2) per unit BET surface area increased linearly from 2 μmol N_2 h^{-1} m^{-2} (MgO) to 51 μmol h^{-1} m^{-2} (Ni–MgO, Ni 50.0 atom%), and then gradually decreased to 22 μmol h^{-1} m^{-2} (NiO). The presence of nickel at the catalyst surface is essential for increased N_2O decomposition, but an excess of nickel ($>$ 50 atom%) was detrimental to the performance of the catalyst.

Normalized Ni K-edge XANES spectra for Ni–MgO catalysts and NiO are shown in Fig. 1A.[5] The rising edge was always within 8339.4–8339.8 eV, demonstrating the valence state of nickel was +2 in the range of Ni 1.5–100 atom%. As the nickel content increases, the two peaks at 8342 and 8355 eV gradually decreased. The peaks at 8362 and 8389 eV for Ni 1.5 atom% [Fig. 1A(a)] gradually shifted, and finally reached 8365 and 8398 eV, respectively, for NiO [Fig. 1A(f)]. The peak intensity at 8389–8398 eV gradually decreased.

These experimental spectra were compared to XANES data generated by *ab initio* calculations. A code FEFF8 was applied to fcc-based model clusters within 6.0 Å from the absorbing Ni atom in self-consistent field (SCF) and multiple scattering calculation modes.[6,7] The imaginary optical potential used in the calculations of the exchange-correlation potential was fixed to 1.5 eV. The XANES spectrum was generated for an isolated Ni^{2+} model which contains only one Ni^{2+} ion at the center of a MgO cluster matrix (Fig. 1B, solid line). The peaks at 8342, 8349 (main peak) and 8389 eV in the XANES of Fig. 1A(a) (Ni 1.5 atom%) were reproduced in the spectra by FEFF8, but the calculated peak at 8359 eV did not correspond to any peaks in Fig. 1A. The gradual decrease in the peaks at 8342 and 8389 eV with increase of Ni^{2+} content was reproduced by FEFF8 (Fig.
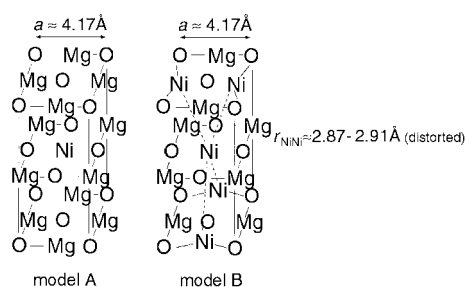
Scheme 1 Ni–MgO models. Model A: Ni 25 atom% unit cell model. Model B: Ni 50 atom% unit cell model. Half of the unit cell is drawn for B. All XANES calculations using FEFF8 were performed for complete (undistorted) fcc coordinates.
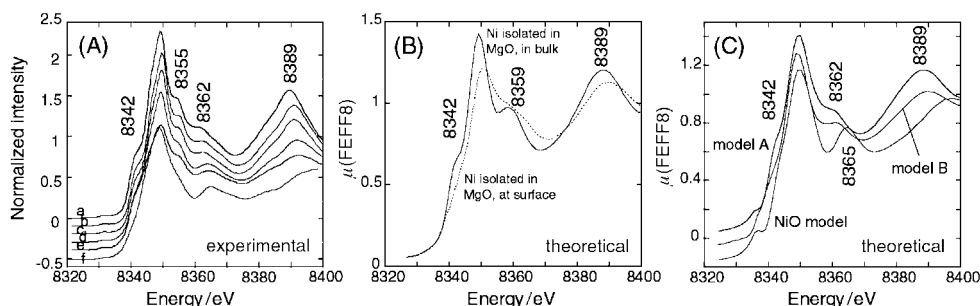
Fig. 1 (A) Ni K-edge XANES for Ni–MgO for Ni atom% of 1.5(a), 4.4(b), 9.5(c), 33.6(d) and 50.0(e) as well as for NiO(f). (B), (C) Ni K-edge XANES generated by FEFF8 for Ni^{2+} isolated in MgO (B, —) or at surface of MgO (B, -----), models A and B and for NiO (C).

Table 1 Ni K-edge EXAFS curve fitting results for Ni–MgO catalysts and NiO

Entry	Ni atom%	Ni–O			Ni···Mg			Ni···Ni			$R_f{}^a$
		N	R/Å	$\Delta(\sigma^2)/10^{-3}$ Å²	N	R/Å	$\Delta(\sigma^2)/10^{-3}$ Å²	N	R/Å	$\Delta(\sigma^2)/10^{-3}$ Å²	
a	1.5	4.7 (±1.2)	2.105 (±0.005)	0.17 (±0.93)	12.0 (±2.8)	2.971 (±0.003)	2.6 (±1.4)				1.9
b	4.4	4.9 (±1.2)	2.086 (±0.005)	0 (±1.1)	11.2 (±1.4)	2.95 (±0.02)	−0.4 (±1.7)	1.0 (±0.8)	2.94 (±0.01)	−2.2 (±3.2)	0.92
c	9.5	6.0 (±0.8)	2.087 (±0.004)	1.1 (±0.8)	10.0 (±1.2)	2.92 (±0.02)	0.2 (±1.3)	2.2 (±0.9)	2.91 (±0.04)	0.3 (±5.4)	1.7
d	33.6	5.1 (±0.9)	2.088 (±0.005)	1.0 (±1.0)	7.6 (±1.8)	2.918 (±0.007)	0 (±1.2)	4.1 (±1.5)	2.91 (±0.02)	5.8 (±2.5)	1.4
e	50.0	4.8 (±1.1)	2.086 (±0.003)	5.3 (±1.9)	7.8 (±2.0)	2.91 (±0.01)	−1.3 (±2.2)	4.4 (±1.3)	2.872 (±0.007)	7.0 (±3.2)	0.71
f	NiO	5.2	2.093	1.0				12.1	2.954	2.8	1.2
g^b	NiO	(6)	(2.089)					(12)	(2.954)		

^{a} $R_f = \int |k^3\chi(\text{obs.}) - k^3\chi(\text{fit})|^2 dk / \int |k^3\chi(\text{obs.})|^2 dk.$ ^{b} According to X-ray crystallography.

1B and C). The peak at 8359 eV in Fig. 1B shifted to 8362 eV for models A and B (Scheme 1) and then to 8365 eV for the NiO model (Fig. 1C).

Based on these trends (peak position and intensity), the local structure of Ni^{2+} in Ni–MgO (Ni 1.5 atom%) corresponds to model A. The experimental spectra for Ni–MgO (Ni 4.4 and 9.5 atom%) were similar to theoretical XANES for model B. The spectra for Ni 33.6 and 50.0 atom% [Fig. 1A(d), (e)] were more similar to theoretical XANES for model B than that for NiO (Fig. 1C). Each peak in the theoretical XANES spectra for the surface isolated Ni^{2+} model was smeared out (Fig. 1B, dotted line), and did not resemble any spectra in Fig. 1A. Hence, impregnated nickel appears to be distributed statistically inside the MgO matrix and less appears at the MgO surface. Although imaginary optical potential values and Debye–Waller factors were varied, the shoulder peak at 8355 eV in Fig. 1A was not reproduced in theoretical XANES spectra.[8]

Ni K-edge EXAFS spectra for Ni–MgO catalysts were analyzed.[9] The model parameters of Ni-O, Ni···Mg, and Ni···Ni bonds were generated by FEFF8 in SCF mode. The application of SCF FEFF8 parameters to this system was validated by the curve fit for NiO (Table 1 entry f) which was in accord with crystallographic data (entry g).[10] The coordination number had an error of 12–26% for Ni–O and Ni···Mg and an error of 30–80% for Ni···Ni due to the fit procedure and FEFF theoretical parameters. For Ni–MgO catalysts, the best fit results and fit errors based on 10–20 relatively good fits (R_f < 2.0%) for each spectrum are listed in Table 1. Obtained Ni–O and Ni···Mg distances for Ni 1.5 atom% indicate the same or slightly smaller (<0.007 Å) coordination distance compared to the pure MgO framework (a = 4.2112 Å). Ni–MgO, (Ni 1.5 atom%) corresponds to either model A (Scheme 1) or an isolated single Ni^{2+} atom model in bulk MgO, in both cases there is no second shell Ni···Ni bond.

With an increase of Ni content above 4.4 atom%, $N_{\text{Ni–O}}$ and $r_{\text{Ni–O}}$ remained almost constant while the $N_{\text{Ni···Ni}}/N_{\text{Ni···Mg}}$ ratio gradually increased (Table 1, entries b–e). Model B (Scheme 1) has eight Ni···Mg and four Ni···Ni bonds, corresponding to Table 1, entries d and e. XANES generated for a model with one to two Ni^{2+} at next-nearest sites (intermediate between models A and B) was similar to XANES generated for model B (four next-nearest Ni^{2+}), consistent with obtained local coordination by EXAFS (Table 1, entries b and c). The value of a according to XRD monotonously decreased from 4.211 ± 0.002 Å (Ni 4.4 atom%) to 4.190 ± 0.001 Å (Ni 50.0 atom%).[11] When the Ni^{2+} ion concentration is nearly one per unit cell (Ni–MgO, Ni 4.4 atom%), the Ni^{2+} site is locally contracted in an undistorted cell with $a \approx 4.17$ Å. With two Ni^{2+} ions per unit cell (Ni–MgO, Ni 33.6 and 50.0 atom%), the Ni^{2+} sites are locally contracted and distorted in the direction of Ni···Mg and Ni···Ni (2.87–2.92 ± 0.02 Å), smaller than $\sqrt{2}r_{\text{Ni–O}}$ [2.950–2.953 (±0.007 Å)] by 0.03–0.08 Å.

Models with locally contracted Ni^{2+} sites (Table 1, entries c–e) shows significantly different Ni···Mg and Ni···Ni distances (2.97–2.94 Å) in the whole range of Ni (0.02–100 atom%) of ref 12. The lower calcination temperature of Ni–MgO samples (773 K)[12] may be the reason for this discrepancy, compared to the temperature of 1173 K used in this work and 1473 K in ref 3. Solid solution formation from supported NiO particles over MgO was suggested to proceed at >1073 K.[2]

The reason for the dependence of N$_2$O decomposition rates on Ni^{2+} content in catalysts can be addressed based on the determined Ni^{2+} local structure. Contracted Ni^{2+} sites at the surface are responsible for the dissociation of the N$_2$–O bond. As the nickel content increases, the number of contracted Ni^{2+} site increases and therefore the N$_2$ formation rate per unit BET surface area increases to Ni 50 atom%. The next elementary step, O(ads) + O → O$_2$, relates to the activity decrease above Ni 50 atom%. An isotope study utilizing ^{18}O labeling of the catalyst surface and ^{16}O(ads) resulted in exclusive ^{16}O^{18}O formation, i.e. the step O(ads) + O(surf) → O$_2$. The Ni^{2+} local coordination for a Ni content of 50.0 atom% (Table 1, entry e) corresponds to model B (Scheme 1). The rate of ^{16}O^{18}O formation was in the order, Ni–MgO (Ni 50.0 atom%) > MgO > NiO, suggesting that surface oxygen bonded to Mg^{2+} is more reactive and diagonal distortion of Ni···Mg and Ni···Ni destabilizes lattice oxygen. The nitrous oxide adsorption was weak and not detected by FTIR. Raman and IR spectroscopy may give further insight of distorted lattice vibration around doped Ni^{2+}.[13]

Notes and references

1 M. Shelef, *Chem. Rev.*, 1995, **95**, 209.
2 F. Arena, B. A. Horrell, D. L. Cocke, A. Parmaliana and N. Giordano, *J. Catal.*, 1991, **132**, 58.
3 A. Kuzmin, N. Mironova, J. Purans and A. Sazanov, *Phys. Status Solidi A*, 1993, **135**, 133.
4 Y. Izumi, K. Oshihara and K. Aika, *Chem. Lett.*, 1998, 727.
5 Spectra were measured at the KEK-PF, 7C (99G259) using an Si(111) double crystal monochromator in transmission mode at 290 K.
6 A. L. Ankudinov, B. Ravel, J. J. Rehr and S. D. Conradson, *Phys. Rev. B*, 1998, **58**, 7565.
7 J. J. Rehr, J. Mustre de Leon, S. I. Zabinsky and R. C. Albers, *J. Am. Chem. Soc.*, 1991, **113**, 5135.
8 Theoretical difficulties in incorporating the experimental effects of beamline energy resolution may be the reason for this result.
9 T. Yokoyama, H. Hamamatsu and T. Ohta, EXAFSH 2.1, The University of Tokyo.
10 A. Corrias, G. Mountjoy, G. Piccaluga and S. Solinas, *J. Phys. Chem. B*, 1999, **103**, 10 081.
11 Based on (111), (200), (220), (311) and (222) reflections.
12 T. Yoshida, T. Tanaka, H. Yoshida, T. Funabiki and S. Yoshida, *J. Phys. Chem.*, 1996, **100**, 2302.
13 J. M. Stencel, *Raman Spectroscopy for Catalysis*, Van Nostrand Reinhold, New York, 1990.